Spectral Dependence of Nanocrystal Photoionization Probability: The Role of Hot-Carrier Transfer

Lazaro A. Padilha, István Robel, Doh C. Lee, Prashant Nagpal, Jeffrey M. Pietryga, and Victor I. Klimov*

Center for Advanced Solar Photophysics, C-PCS, Chemistry Division, Los Alamos National Laboratory, Los Alamos, New Mexico 87545, United States

ABSTRACT We conduct measurements of photocharging of PbSe and PbS nanocrystal quantum dots (NQDs) as a function of excitation energy ($\hbar\omega$). We observe a rapid growth of the degree of photocharging with increasing $\hbar\omega$, which indicates an important role of hot-carrier transfer in the photoionization process. The corresponding spectral dependence exhibits two thresholds that mark the onsets of weak and strong photocharging. Interestingly, both thresholds are linked to the NQD band gap energy (E_g) and scale as $\sim 1.5E_g$ and $\sim 3E_g$, indicating that the onsets of photoionization are associated with specific nanocrystal states (tentatively, 1P and 2P, respectively) and are not significantly dependent on the energy of external acceptor sites. For all samples, the hot-electron transfer probability increases by nearly 2 orders of magnitude as photon energy increases from 1.5 to 3.5 eV, although at any given wavelength the photoionization probability shows significant sample-to-sample variations ($\sim 10^{-6}$ to 10^{-3} for 1.5 eV and $\sim 10^{-4}$ to 10^{-1} for 3.5 eV). In addition to the effect of the NQD size, these variations are likely due to differences in the properties of the NQD surface and/or the number and identity of external acceptor trap sites. The charge-separated states produced by photoionization are characterized by extremely long lifetimes (20 to 85 s) that become longer with increasing NQD size.

KEYWORDS: photoionization · nanocrystals · charge separation · trapping · carrier multiplication · photoluminescence · Auger recombination

Photocharging of nanocrystal quantum dots (NQDs) is a process in which the inorganic nanocrystal core acquires a net charge upon absorption of one or more photons. As a whole, the NQD may still remain neutral, as the charge removed from the core could reside either in some surface defect site or in a trap within the ligand shell. Photocharging has been invoked in earlier spectroscopic studies of these structures to explain observations such as photodarkening[1] and fluorescence intermittency.[2,3] For many optical applications of NQDs, such as in lasing, fluorescent biological labeling, and solid-state lighting, photocharging has been considered an undesirable process, as it reduces photoluminescence (PL) quantum yields by enhancing the rate of nonradiative carrier recombination via the Auger process.[4] Photocharging also complicates the analysis of spectroscopic data, especially in the case of time-resolved studies of carrier multiplication (CM) or multiexciton generation, a process in which absorption of a single photon produces two or more excitons.[5−8]

Photocharging has been investigated most frequently in NQDs immobilized on substrates,[9−11] while only a few recent studies have focused on solution samples.[7,8] Recently, McGuire *et al.*[5,6,8] and Midgett *et al.*[7] investigated the effect of photocharging on spectroscopic measurements of CM using transient absorption and time-resolved PL. These studies were conducted on well-passivated colloidal PbSe NQDs and indicated that photocharging affects CM measurements even at very low excitation intensities. Further, it was found that photocharging occurs mostly under ultraviolet (UV) excitation and that the lifetime of the charged state was on the order of tens of seconds,[7,8] many orders of magnitude longer than single- or multiexciton recombination times in these materials. The probability of photocharging following a photon absorption event derived from these studies was relatively low, on the order of 10^{-3}–10^{-4} for 3 eV excitation.[7,8] However, despite the small likelihood of photocharging by a single absorbed photon, the very long lifetimes of charge-separated states facilitate the buildup of an appreciable population of charged species (up to more than 10% of all NQDs residing in a photoexcited volume) in the course of a prolonged exposure to incident radiation.

The studies of ref 8 indicate that, while well-passivated samples may exhibit significant photocharging under UV (~3 eV) excitation, they typically do not show any signatures of photocharging when excited with infrared (~1.5 eV) photons. These results imply that photocharging in these NQDs occurs via direct ejection of a hot carrier *prior to its relaxation to the band-edge*. This further indicates the direct relevance of

* Address correspondence to klimov@lanl.gov.

Received for review March 25, 2011 and accepted May 17, 2011.

Published online May 17, 2011
10.1021/nn201135k

studies of UV-light-induced photocharging to the problem of hot-electron extraction, a topic of significant interest from the points of view of both fundamental understanding of hot-carrier dynamics[12,13] and potential applications of this process in generation-III architectures for solar-energy conversion.[14,15]

Studies of photocharging also directly relate to the problem of photoionization in "real-life" NQD samples in which the semiconductor nanocrystals are surrounded by a shell of organic ligands and dispersed in solutions or solid matrices or assembled into films. Traditionally, photoionization refers to the removal of an electron from a given material to a zero-energy vacuum state by a photon of sufficient energy. In semiconductors, the characteristic energy of this process (the "ionization energy") corresponds to the energy separation between the top of the valence band and the vacuum level. In the case of NQD samples, the incident photon can effectively eject the electron from the nanocrystal by promoting it not necessarily to the vacuum level, but to some acceptor state within the ligand shell or the solvent/matrix. In addition, another scenario is the ejection of a hole from the NQD via the intercession of an electron-donating species outside the nanocrystal. Both of these processes will lead to photocharging of the NQD and are referred to here as "photoionization", although, as was noted above, this type of photoionization is different from the one traditionally considered in condensed matter physics. Consequently, the characteristic energies of photoionization in "real-life" NQD samples may differ significantly from the textbook ionization energies.

In this study, we use spectrally and temporally resolved measurements of photocharging in solutions of PbSe and PbS NQDs as a tool to quantify the photoionization thresholds and hot-carrier transfer probabilities as a function of pump photon energy. The spectral dependence of photocharging reveals two photoionization thresholds associated with onsets of what we will refer to as weak and strong photocharging. Both of these thresholds show direct correlations with the NQD band gap energy (E_g) and scale as $\sim 1.5E_g$ and $\sim 3E_g$. This behavior is not well described by the traditional picture of ionization involving the final vacuum state and instead indicates that the onset of hot-carrier transfer is associated with a specific NQD state (tentatively, 1P) and is only weakly dependent on the energy of the acceptor site outside the nanocrystal. Interestingly, the $\sim 3E_g$ onset for strong ionization (assigned tentatively to the 2P state) is close to the thresholds reported for CM in these materials, which calls for special caution in the case of experimental studies where the presence of CM is inferred solely on the basis of spectral dependences without quantitative measurements of multiexciton yields. In accord with results of refs 7 and 8 we measure very long, tens-of-seconds lifetimes of charge-separated states that provide a time scale of back-transfer of the trapped charge to the NQD. We further observe that these lifetimes become longer with increasing NQD size (*i.e.*, decreasing E_g), which can be rationalized using the configuration-coordinate approach.

Earlier studies[6,8] indicate that only a subset of NQDs is susceptible to photoionization and that this "chargeable" fraction of NQDs in the studied samples is up to ~20%. This suggests that sites that serve as carrier acceptors are not intrinsic to the NQDs but are rather associated with some impurities or defects that are most likely incorporated into the ligand shell. In the present study, we observe that in these "chargeable" nanocrystals, the hot-carrier transfer probability shows a fast growth with excitation energy, and in some samples it reaches a value of ca. 10% for photon energies of ~3.5 eV. For such high probabilities of carrier transfer, photocharging is no longer a weak cumulative effect but rather a highly effective process, which can affect the properties of a large subset of the NQDs immediately following exposure to even a single laser pulse. The high efficiency of hot-carrier transfer found in the present study in the case of incidental acceptors suggests that if it is required by a certain application (*e.g.*, in hot-electron solar cells), the efficiency of this process can be significantly increased by intentionally introducing well-defined acceptor sites with appropriately designed energy levels and acceptor–NQD wave function overlap. The results of this work have direct relevance to studies of multiexciton generation via CM. Specifically, the fact that the spectral dependence of photocharging mimics that expected for CM emphasizes the importance of a careful analysis of the potential effects of photocharging on the results of both spectroscopic studies of CM and photocurrent and photoconductive gain measurements.

RESULTS AND DISCUSSION

To monitor photocharging, we exploit the fact that photoionization suppresses PL. The excitation of a nanocrystal that already has a net charge in its core results in a trion, which can recombine through nonradiative Auger recombination, in which the electron–hole pair decays by transferring its energy to the third charge carrier. Since Auger lifetimes are much shorter than the single exciton radiative lifetimes (sub-ns *versus* hundreds of ns time scales),[8] trions are essentially nonemitting in PbSe and PbS NQDs.

To quantify the degree of photocharging, we compare steady-state PL intensities of a NQD solution recorded under static and stirred conditions. Stirring prevents accumulation of charged species in the excited volume of the sample by continuously refreshing the solution exposed to incident light. Therefore, the steady-state fraction of ionized NQDs, f_s, in the excited

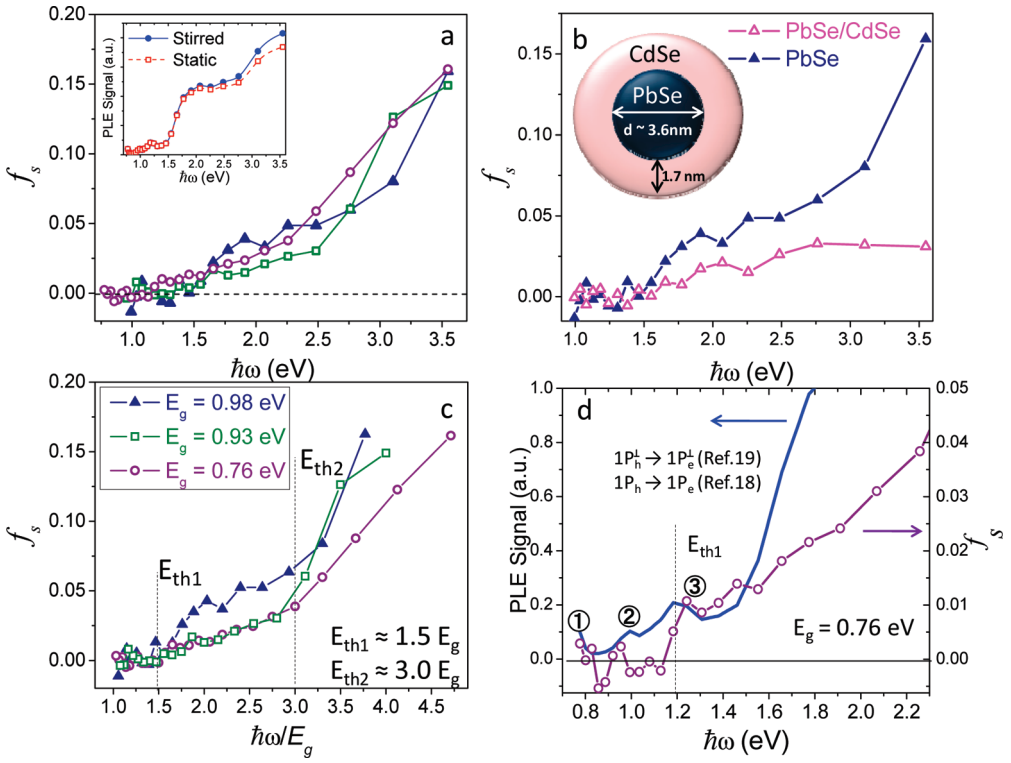

Figure 1. (a) Spectral dependence of the steady-state fraction of ionized PbSe NQDs obtained from the ratio of the static and stirred PLE signals (see example in the inset of panel "a"; sample E_g = 0.76 eV) plotted as a function of photon energy. The data are shown for three PbSe NQD samples: E_g = 0.98 eV (solid blue triangles), E_g = 0.93 eV (open green squares), and E_g = 0.76 eV (open purple circles). (b) Comparison of the photocharging spectra for core-only PbSe and core/shell PbSe/CdSe NQDs with similar band gap energies of 0.98 eV. (c) Same as in "a" but as a function of photon energy normalized by the NQD band gap energy. (d) Comparison of the spectral dependence of the degree of photoionization with the PLE spectrum for PbSe NQDs with E_g = 0.76 eV.

sample can be inferred from the comparison of the PL intensities under stirred (I_{PL}) and static (I^*_{PL}) conditions as $f_s = 1 - I^*_{PL}/I_{PL}$. The spectral dependence of photocharging is investigated by comparing stirred and static PL intensities of a given sample as a function of photon energy using a PL excitation (PLE) setup (details are in the Methods section).

Photoionization Thresholds in Relation to Band Gap Energies. In the inset of Figure 1a, we show an example of "raw" PLE spectra collected for a PbSe NQD sample with E_g = 0.76 eV under static (open red squares) and stirred (solid blue circles) conditions while monitoring the PL intensity at the center of the emission peak. While at low spectral energies the spectra are perfectly overlapping, they show a progressive deviation (static signal becomes smaller than the stirred one) above a certain threshold energy. This deviation is a signature of photocharging due to hot-carrier transfer from the NQD, as was recently reported in ref 8. From the ratio of the PLE signals measured under stirred and static conditions ($r = I_{PL}/I^*_{PL}$) we can derive the degree of steady-state photocharging: $f_s = (r - 1)/r$. The spectral dependence of f_s obtained in this way for three different PbSe NQD samples, shown in the main panel of Figure 1a, consistently suggests contributions from two processes. Weak photoionization occurs above an onset in the near-IR region, while a steeper dependence of the degree of photocharging on photon energy $\hbar\omega$ above a higher-energy threshold in the visible–UV range suggests the onset of strong photoionization. This second threshold indicates an opening of an additional ionization pathway which may be associated with the participation of a new subset of trapping sites that become accessible by an electron or a hole with sufficiently high energy. Another possibility discussed later in the paper is that the higher-energy threshold develops as a result of Auger-assisted ionization associated with the onset of CM.

Further evidence of the existence of two separate photoionization pathways is found in comparative studies of PbSe core-only samples and PbSe/CdSe core/shell heterostructured NQDs with a similar core size (Figure 1b). This core/shell system is of particular interest to the current study, because while the CdSe shell in PbSe/CdSe NQDs effectively confines excited holes to the PbSe core, electrons are significantly delocalized out into the shell.[16,17] While the presence of the shell reduces the degree of photoionization across the entire spectrum, the effect is most significant at energies above E_{th2}, suggesting a selective suppression of the second photoionization pathway. This implies that the first ionization pathway, which is less affected by the

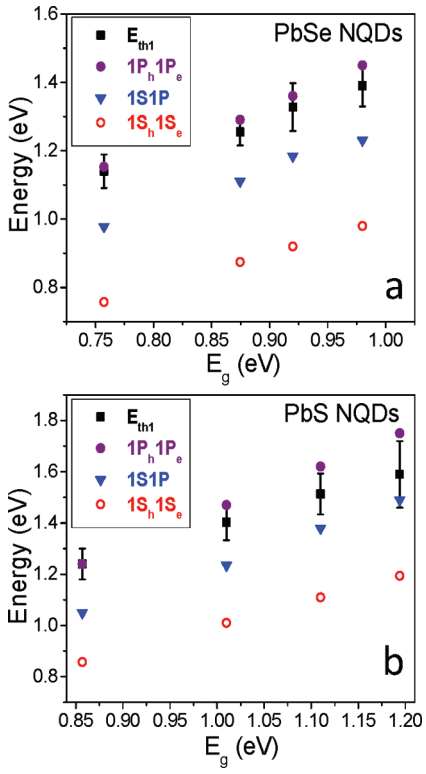

Figure 2. Calculated energies of the parity-allowed $1S_h1S_e$ (open red circles) and $1P_h1P_e$ (solid purple circles) and parity-forbidden 1S1P (solid blue triangles) optical transitions in comparison to the measured energy of the lower-energy ionization threshold E_{th1} (solid black squares) for (a) PbSe NQDs and (b) PbS NQDs.

shell, is likely associated with hot-electron trapping, while the second, highly suppressed pathway involves holes.

Replotting the spectra from Figure 1a in terms of the photon energy normalized by the band gap energy, E_g (Figure 1c), reveals that both the low- and the high-energy thresholds (E_{th1} and E_{th2}) seem to scale with E_g as $\sim 1.5E_g$ and $\sim 3E_g$, respectively, for all samples. The existence of such scaling would be quite unusual if considered from the point of view of traditional photoionization, in which the ionization energy is determined by the energy difference between the NQD and the external acceptor levels. A direct correlation between the photoionization thresholds and E_g suggests that in our samples the onset of charge separation is associated instead with excitation of a specific NQD state, and it is not significantly dependent on the acceptor site energy.

In Figure 1d, we compare the photoionization and the PLE spectra for the PbSe NQD sample with $E_g = 0.76$ eV. We see that the threshold for weak ionization occurs at the same photon energy as the third PLE peak. To identify the NQD states involved in the corresponding transition, we plot the energy E_{th1} as a function of E_g for the PbSe NQD samples from Figure 1 and for four sizes of PbS NQDs (Figure 2a and b, respectively). We further compare these data to the energies of the parity-allowed $1S_h1S_e$ and $1P_h1P_e$ and the parity-forbidden $1P_h1S_e$ and $1S_h1P_e$ transitions calculated using a $k \cdot p$ four-band envelope-wave function formalism developed by Kang and Wise.[18] Since this model assumes mirror symmetry between the conduction and the valence bands of PbSe and PbS, the energies of $1P_h1S_e$ and $1S_h1P_e$ transitions are close to each other; therefore, below we denote these two transitions using the same notation: 1S1P. The $1S_h1S_e$, 1S1P, and $1P_h1P_e$ transitions likely correspond to the PLE peaks 1, 2, and 3 in Figure 1d, respectively. It should be noted that while the model of ref 18 considers isotropic bands to describe the structures of optical transitions in PbSe and PbS NQDs, other models that take into account band anisotropy predict that the second and the third optical transitions are both parity allowed and involve the $1P_h''$/$1P_e''$ and the $1P_h^{\perp}$/$1P_e^{\perp}$ states, respectively.[19,20] Regardless, the calculated energies of these transitions are close to those in ref 18, whose notation will be used in our discussion below.

Interestingly, for both PbSe and PbS nanocrystals we observe a close correspondence between E_{th1} and the energy of the parity-allowed $1P_h1P_e$ transition, suggesting that the onset for photocharging is associated with excitation of a carrier (an electron or a hole) into the 1P state. We also notice that as we consider progressively smaller NQDs, the ionization threshold shifts toward formally parity-forbidden $1P_h1S_e$ and $1S_h1P_e$ transitions, an effect that is even more pronounced for PbS NQDs. This observation can be rationalized by taking into account recent studies by Nootz *et al.*,[21] according to which an increase in the structural asymmetry of an NQD, as is typically seen in smaller-size particles, increases the strength of nominally forbidden transitions. As a result, the likelihood of excitation to the 1P state (from which photocharging may occur) *via* a 1S1P transition should increase with decreasing NQD size. Moreover, the more pronounced shift of E_{th1} toward the 1P1S transition in PbS relative to PbSe NQDs is consistent with previous observations of a stronger effect of symmetry breaking in PbS particles as inferred from the two-photon absorption studies of ref 21.

In a similar manner, calculations using the Kang and Wise model[18] indicate that the higher-energy, $\sim 3E_g$ photoionization threshold is close to the 2P2P allowed optical transition, suggesting that the second photocharging pathway opens when one of the carriers is excited into the 2P state. However, the high density of optical transitions at $\sim 3E_g$ complicates a precise identification of the state associated with E_{th2}.

NQD Size Dependence of Lifetimes of Charge-Separated States. As was proposed in ref 8, by monitoring slow, laboratory time frame dynamics of PL quenching one can directly measure the lifetimes of charge-separated states (τ_{eh}) produced by a hot-carrier-transfer process, *i.e.*, the time required for the trapped charge to return to the core of the NQD. An initial study of temporally

resolved PL quenching indicated very large values of τ_{eh}, on the order of tens of seconds.[8] Similar time scales were observed in ref 7, where photocharging was studied by monitoring transient absorption signals from PbSe NQD solution samples circulated at a variable rate through a flow cell.

We study the dynamics of photocharging through two experiments that allow us to monitor either the development or recovery of PL quenching. In the first, the evolution of PL excited by a single, high-energy source (capable of producing photoionization) is monitored after stirring is abruptly stopped, allowing a population of photoionized NQDs to accumulate. In the second, two independent "excitation" wavelengths are used: a relatively high energy source to produce photoionization in an unstirred sample and a tunable IR source to resonantly excite PL without contributing to photoionization. This allows us to monitor PL recovery when the photoionizing beam is blocked and the NQDs in the static sample return to the uncharged state (see details in the Methods section).

The dynamics of the population of photoionized nanocrystals can be described by the following rate equation:

$$df(t)/dt = [f_0 - f(t)]g_{abs}\gamma - f(t)/\tau_{eh} \quad (1)$$

where f_0 is the fraction of chargeable NQDs in the ensemble,[8] g_{abs} is the excitation rate calculated as $g_{abs} = \sigma w$ (σ is the NQD absorption cross-section at a given photon energy and w is the excitation flux), and γ is the probability of photoionization following a photon absorption event. On the basis of this rate equation, the evolution of $f(t)$ following abrupt termination of stirring (ionizing light is still on) can be described by an exponential growth, $f(t) = f_s(1 - e^{-t/\tau_{eff}})$, where

$$f_s = f_0 g_{abs}[g_{abs} + (\gamma\tau_{eh})^{-1}]^{-1} \quad (2)$$

is the degree of steady-state photocharging and $\tau_{eff}^{-1} = \tau_{eh}^{-1} + \gamma g_{abs}$ is the effective time constant of the buildup of the population of charged species. In the case of low-intensity excitation when $g_{abs} \ll (\gamma\tau_{eh})^{-1}$, and hence, $f_s \ll f_0$ (which is the regime probed in our dynamical studies), eq 2 reduces to $f_s = f_0 g_{abs}\gamma\tau_{eh}$, while τ_{eff} becomes equal to τ_{eh}. Under these conditions, the time dependence of the PL signal (*i.e.*, the PL decay) is described by $I_{PL}(t) = I_s[1 - f_s(e^{-t/\tau_{eh}})]$, where I_0 is the PL intensity in a nonionized sample for which $f_s = 0$. Using the rate equation for $f(t)$, we can also show that the growth of the PL intensity due to decay of charge-separated species when exposure to ionizing light is stopped is described by $I_{PL}(t) = I_0(1 - f_s e^{-t/\tau_{eh}})$. These two expressions indicate that the dynamics of both PL decay (observed when stirring is abruptly stopped) and PL recovery (observed when the source of ionizing light is blocked) are determined by the lifetime of charge-separated states, τ_{eh}, while the relative change in the PL intensity is determined by the steady-state fraction of ionized nanocrystals f_s.

To detect any size dependence in τ_{eh} lifetimes, we have studied transient PL quenching in the same four PbSe NQD samples mentioned above. In order to obtain more detailed information on the size dependence of τ_{eh}, for each sample we measure PL dynamics at several different wavelengths within the inhomogeneously broadened PL band; these measurements correspond to probing differently sized subsets in a NQD ensemble.

Figures 3a and 3b show slow PL transients recorded for two PbSe NQD samples (E_g = 0.98 eV and E_g = 0.76 eV, respectively) by monitoring either the buildup of charge-separated species (Figure 3a) or their decay (Figure 3b). Generally, τ_{eh} becomes shorter with decreasing NQD size; a similar trend is exhibited by all other studied samples, as seen from the summary of lifetime measurements in Figure 3c (3.08 eV excitation). The measured data points form a "universal" size dependence, which does not "break" between different samples. This might imply that the acceptor site involved in the photoionization process is associated with some state within the ligand shell (as was originally proposed in ref 8), and this state is not significantly influenced by extrinsic factors, such as synthesis-induced variations in degree of surface coverage or the identity of the solvent molecules.

Because of the potential difference between "weak" and "strong" photoionization processes, we also studied the effect of excitation wavelength on the lifetime of charge-separated states. In Figure 3d, we compare PL transients recorded for a PbSe NQD sample with E_g = 0.98 eV using 2.33 and 3.08 eV excitation wavelengths, respectively, corresponding to excitation below and above the second threshold for photoionization. These data show that the lifetime of charge-separated states produced by 2.33 eV photons is, indeed, shorter than that for the 3.08 eV excitation. This result is consistent with the explanation that the second threshold is associated with a distinct ionization pathway, which involves trap sites that are likely more strongly decoupled from the NQD excitations and are therefore characterized by longer lifetimes.

To model the size-dependent trend in Figure 3c, we have used a configuration-coordinate approach outlined in ref 8 and previously applied, for example, to treat the problem of intraband relaxation in quantum dots *via* coupling to external defects.[22] While at present we cannot conclusively identify the type of carrier transferred from the nanocrystal during photoionization, for the sake of this illustration we will discuss photocharging in terms of electron transfer. We further focus on the problem of back transfer from the external trap center to the NQD valence band. Given a very low probability of this process (tens of second lifetimes of charge-separated states), we can treat it assuming a

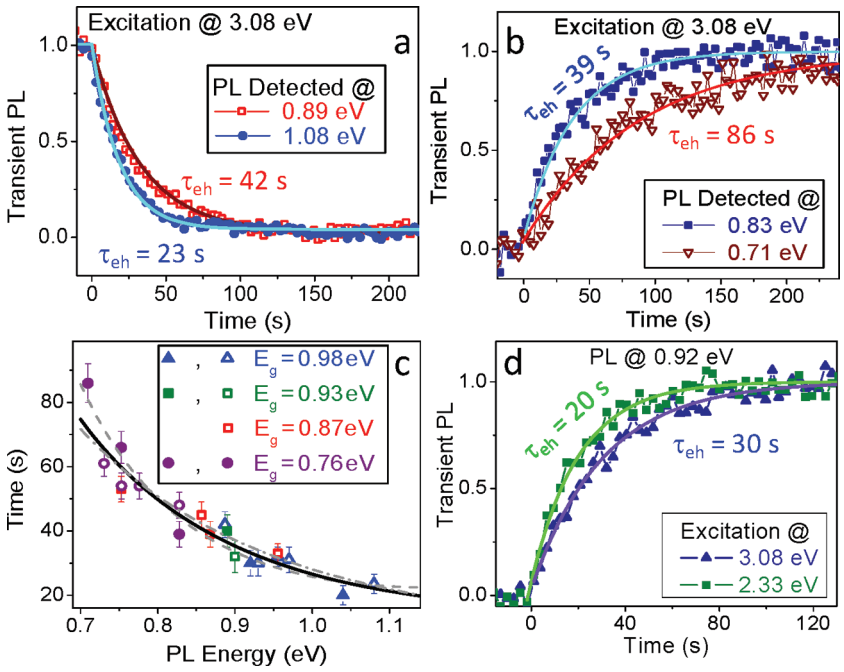

Figure 3. (a) Lifetime measurements of charge-separated states generated by 3.08 eV excitation of PbSe NQD sample with E_g = 0.98 eV (symbols); measurements are conducted at two different PL energies, 1.08 eV (solid blue circles) and 0.89 eV (open red squares), by monitoring dynamics of PL quenching after stirring is abruptly stopped. The lines are single-exponential fits to the data. (b) Measurements of τ_{eh} for PbSe NQD sample with E_g = 0.76 eV by monitoring the recovery of PL after the ionization source at 3.08 eV is blocked; PL monitored at either 0.83 eV (solid blue squares) or 0.71 eV (open red triangles). The lines are single-exponential fits to the data. (c) Summary of the τ_{eh} measurements for four different PbSe NQD samples (3.08 eV excitation) as a function of NQD band gap energy. The open (solid) symbols correspond to the measurements of the buildup (decay) of charged species. The lines are fits to the configuration-coordinate model using three different sets of parameters $S\hbar\Omega$ and E_0: $S\hbar\Omega$ = 0.80 eV and E_0 = 0.45 eV (solid line), $S\hbar\Omega$ = 0.35 eV and E_0 = 0.14 eV (dashed line), and $S\hbar\Omega$ = 1.50 eV and E_0 = 0.95 eV (dashed-dotted line). (d) Dynamics of PL recovery due to decay of charge-separated species for two different wavelengths of the ionization source, 3.08 eV (solid blue triangles) and 2.33 eV (solid green squares), fit to a single-exponential growth (lines); PbSe NQDs with E_g = 0.98 eV.

weak-coupling, nonadiabatic regime for which the rate $W_{eh} = 1/\tau_{eh}$ can be expressed as $W_{eh} = (\Omega/2\pi)P_{T,V} \exp(-(\Delta E_{T,V}/k_BT))$, where Ω is the frequency of trap center vibrations, $P_{T,V}$ is the wave function overlap-dependent factor describing the strength of trap coupling to the NQD valence band state, and $\Delta E_{T,V}$ is the respective potential barrier (Figure 4).

While changing NQD size can, in principle, affect both $P_{T,V}$ (through the change in the leakage of the electron wave function outside the dot) and $\Delta E_{T,V}$ (through confinement-induced shift of the valence-band states), here we concentrate on the effect of a varying potential barrier on the back-transfer rate. On the basis of the configuration-coordinate diagram in Figure 4 we can obtain the following expression for $\Delta E_{T,V}$:

$$\Delta E_{T,V} = \frac{\hbar\Omega S}{4}\left(\frac{E_0+\delta}{\hbar\Omega S} - 1\right)^2 \qquad (3)$$

where E_0 is the trap-site energy at the bottom of the vibrational well (configuration coordinate $Q = Q_0$; see Figure 4 for notations) measured with regard to the top of the valence band in the largest nanocrystals used in the study (E_g = 0.76 eV), S is the Huang−Rhys factor defined as $S = Q_0^2/2$, and δ is the valence band shift due to quantum confinement in samples of smaller sizes. The latter value is obtained from the change in the band gap energy (ΔE_g) assuming that because of mirror symmetry between the conduction and the valence bands in PbSe and PbS, the confinement-induced shifts are identical for electrons and holes, and hence, $\delta = \Delta E_g/2$. The lifetime of the charge-separated state can be then written as $1/\tau_{eh} = (1/\tau_0) \exp(-(\Delta E_{T,V}/k_BT))$, where τ_0 is the time constant that corresponds to the back transfer rate observed when $\Delta E_{T,V} = 0$.

Using eq 3, we can closely describe the measurements in Figure 3c. However, due to a relatively small range of energies studied in our experiments, we cannot determine unique values of $\hbar\Omega S$ and E_0 from the fitting procedure. Instead, we obtain a fairly broad range of values ($\hbar\Omega S$ can vary from 0.35 to 1.5 eV and, correspondingly, E_0 from 0.14 to 0.95 eV) that produce a reasonably good fit to the experimental data (lines of different styles in Figure 3c). The studies of a wider range of NQD sizes as well as temperature-dependent measurements should, in principle, help one to reduce the uncertainty in the values of $\hbar\Omega S$ and E_0. These studies are currently in progress.

Spectral Dependence of Photoionization Probabilities. Previously, McGuire *et al.*[8] showed that by analyzing

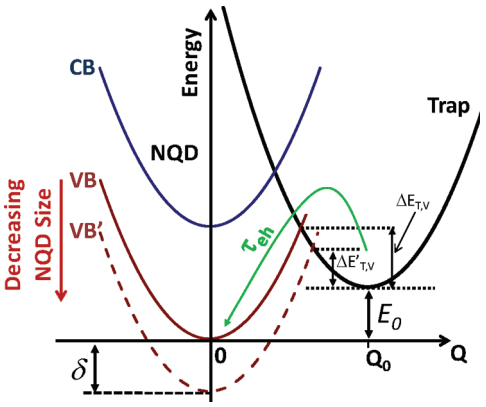

Figure 4. Configuration-coordinate diagram used in the analysis of the NQD size dependence of the lifetimes of charge-separated states. The black and the colored parabolas correspond, respectively, to electronic states of the external trap center and the NQD. Q_0 is the "displaced" configuration coordinate of the center following electron transfer. The solid and the dashed brown lines show schematically the valence-band-edge hole states for larger and smaller NQDs, respectively. Corresponding potential barriers that control the back-transfer rate of the trapped electron are denoted as $\Delta E_{T,V}$ and $\Delta E'_{T,V}$. As the NQD size is reduced, the height of the potential barrier decreases ($\Delta E'_{T,V} < \Delta E_{T,V}$), which leads to shortening of τ_{eh}.

the excitation-rate dependence of the degree of photocharging, one can determine both f_0 and the product $\gamma\tau_{eh}$. This analysis is based on eq 2, according to which f_0 defines the steady-state saturation value of f_s while $(\gamma\tau_{eh})^{-1}$ corresponds to the pump-intensity onset of photocharging saturation. Here, we use the pump-intensity-dependent studies of f_s, along with the spectral dependence of f_s derived from PLE measurements (Figure 1) and the results of τ_{eh} measurements, to map the spectral dependence of the probability of photocharging γ. Below, we illustrate this procedure by applying it to a sample of PbS NQDs with E_g of 1.18 eV.

In Figure 5a, we show the dependence of f_s on excitation rate for four different pump photon energies. By fitting these data to eq 2, we determine f_0 (the fraction of "chargeable" NQDs) for each $\hbar\omega$. Interestingly, for the three lower photon energies (1.91, 2.26, 3.08 eV), we obtain the same value of f_0 of ~8%. However, for excitation at 3.55 eV, f_0 increases up to 13%, indicating the increase in the number of chargeable nanocrystals. Together with observations of a faster growth of f_s above E_{th2} (Figure 1) and the dependence τ_{eh} on excitation wavelength (Figure 3d), the increase in f_0 at higher spectral energies is a further piece of evidence indicating the opening of an additional ionization pathway above the second, higher-energy photocharging threshold.

From the onset of saturation of f_s, we can determine the product of $\gamma\tau_{eh}$, which is plotted in Figure 5b as a function of $\hbar\omega$ (red open circles). In the same plot, we also show a larger set of data (black solid triangles) obtained from the static-*versus*-stirred PLE measurements. Since PLE studies were conducted in the low-intensity regime, for which $f_s \propto g_{abs}$, $\gamma\tau_{eh}$ can be derived from the expression $\gamma\tau_{eh} = f_s (f_0 g_{abs})^{-1}$ using f_0 from fits to the data in Figure 5a.

The values of $\gamma\tau_e$ obtained from the PLE studies closely agree with results derived from pump-intensity dependences in Figure 5a and display two ionization thresholds, one at 1.75 eV (weak ionization) and the other at 3.1 eV (strong ionization). Using the results of τ_{eh} measurements, we can further calculate the spectral dependence of γ, which is shown in Figure 5c. These data indicate that probability of photoionization is nonzero (~10^{-3}) even at low energies (~1.1−1.7 eV). Above the first threshold of ~1.75 eV, it increases to ~0.02−0.03 and then further to ~0.06−0.08 (*i.e.*, ~6−8%) above the second, ~3.1 eV threshold. The latter value, however, should be treated with caution, as it likely underestimates the actual probability of photocharging. In the case of large γ values that approach f_s, our procedure for deriving γ introduces a systematic error because even in the case of stirring, sample emission is reduced compared to the ideal situation where $f_s = 0$, as there is a significant probability of photoioization following a single-photon absorption event. As a result, the apparent degree of photocharging derived from the ratio of the static and the stirred emission efficiencies is smaller than the actual value of f_s, which may further lead to the underestimation of γ.

The fast growth of γ with $\hbar\omega$ is observed for all other PbSe and PbS NQDs studied; however, the absolute values of γ differ significantly from sample to sample. An example of significantly smaller probabilities of photocharging is shown in Figure 5d for a lower band gap sample of PbSe NQDs (E_g = 0.87 eV). In this case, at low photon energies ($\hbar\omega$ < 1.3 eV) γ is on the order of 10^{-5} and eventually increases to ~3×10^{-3} at 3.5 eV. These values are close to those reported previously in ref 8 for PbSe NQDs.

A large sample-to-sample variability in the degrees of photocharging even between nominally identical samples was pointed out in our earlier studies in refs 6 and 8, where the effect of photocharging on apparent CM yields was analyzed. This difference was attributed to uncontrolled variations in the composition of the surface passivation layer, which could lead to a varying number and/or identity of acceptor sites within the ligand shell. One can also anticipate more systematic trends due to changes in the NQD size (*i.e.*, band gap energy). It is expected that a decrease in NQD size increases the leakage of the electronic wave function outside the NQD, which should lead to increased coupling of NQD excitations to external acceptors and, hence, the increased probability of charge transfer. Therefore, in addition to differences in surface properties, the size effect is also likely a factor, which

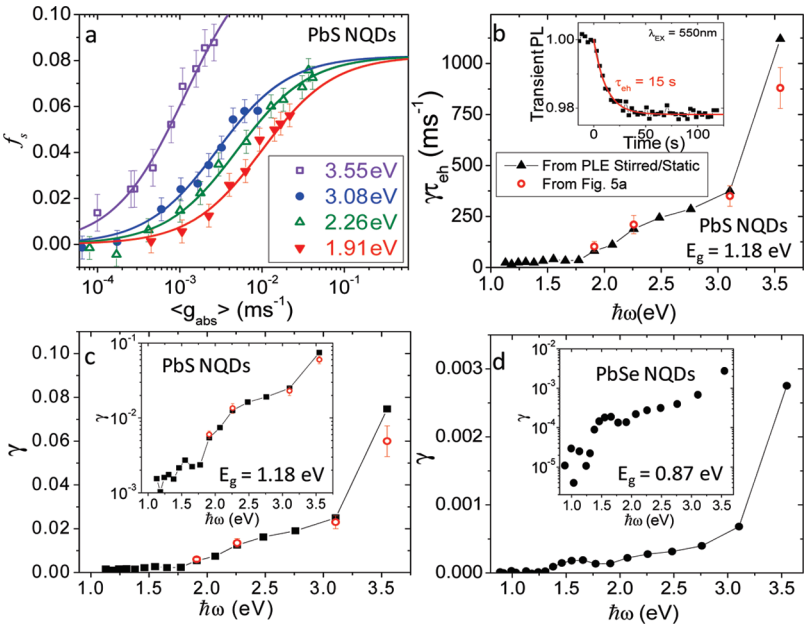

Figure 5. (a) Steady-state fraction of charged NQDs (symbols) as a function of excitation rate measured for four different excitation photon energies (indicated in the legend) fit to the model described by eq 2 (lines); sample with E_g = 1.18 eV. For excitation at 3.55 eV, the fitting procedure produces f_0 = 0.13 and $\gamma\tau_{eh}$ = 880 ms. For three other excitation wavelengths, the fits yield the same value of f_0 = 0.082 but three different values of $\gamma\tau_{eh}$ = 350 ms (3.08 eV), 200 ms (2.26 eV), and 100 ms (1.91 eV). (b) Spectral dependence of $\gamma\tau_{eh}$ obtained from the static *vs* stirred PLE measurements (solid black triangles); these data are in excellent agreement with results derived from the analysis of the excitation-rate dependences in panel "a" (shown in "b" by open red circles). (c) Photoionization probability derived from the data in panel "b" as a function of $\hbar\omega$. Inset: same but in the logarithmic representation. This is an example of high photoionization probabilities that reach the value of ~0.06−0.08 (*i.e.*, ~6−8%) at 3.5 eV. (d) Same as in "c" but for PbSe NQD sample shown in both linear (main panel) and logarithmic (inset) representations. This is an example of the sample with much lower ionization probabilities that reach only the value of 0.0028 (*i.e.*, 0.28%) at 3.5 eV.

leads to a greater probability of photocharging in the wider-band gap sample in Figure 5c compared to the lower-band gap NQDs in Figure 5d.

Relation to Studies of Carrier Multiplication. The results of the present work have direct relevance to studies of CM. As was first pointed out in ref 5 and analyzed in great detail in refs 6 and 7, uncontrolled photocharging can significantly complicate quantitative measurements of CM yields by exaggerating the Auger-decay signatures of multiexcitons. Recently, this issue was addressed theoretically in ref 23. A deleterious effect of surface trapping on measurements of CM and Auger recombination was also discussed in ref 24.

The present studies re-emphasize the importance of carefully accounting for the effects of photocharging during CM measurements, as signatures of charged species produced by photoionization can be easily misinterpreted as CM signatures (especially without a careful lifetime analysis to distinguish, *e.g.*, between trions and biexcitons). For example, inspection of the data in Figure 1 indicates that the spectral dependences of photocharging closely mimic those expected for CM: specifically, photoionization exhibits a well-defined threshold above which the degree of photocharging shows a continuous growth with $\hbar\omega$. Especially deceiving in experimental measurements can be the fact that the spectral onset of strong photocharging scales with the band gap energy (as expected for CM) and is coincidentally near the threshold for CM observed experimentally (~2.5−3E_g).[5,25]

Because of the close correlation between the two thresholds, we have considered the possibility that the onset for strong photocharging develops as a result of Auger-assisted ionization associated with CM. The physics underlying this effect is based on Auger decay of multiexcitons produced by CM. A carrier excited in the Auger recombination event can access a larger number of potential trap sites outside the nanocrystal, which might increase the probability of photocharging in the multiexciton state compared to the single-exciton state (see schematics in Figure 6a). Previously, Auger-assisted photoionization was used to explain PL degradation in nanocrystals grown in glass matrices[26] and invoked to rationalize NQD behaviors in single-nanocrystal studies of PL intermittency ("PL blinking").[3,27] This process was also directly observed in transient absorption[28] and time-resolved PL[29] measurements of NQD ensemble samples. More recently, Auger-assisted ionization was used to explain a rapid growth of photoconductive gain in PbS NQD-based device structures at high photon energies.[30] The fact that the spectral onset of this effect correlated with the band gap energy was considered a signature of CM.

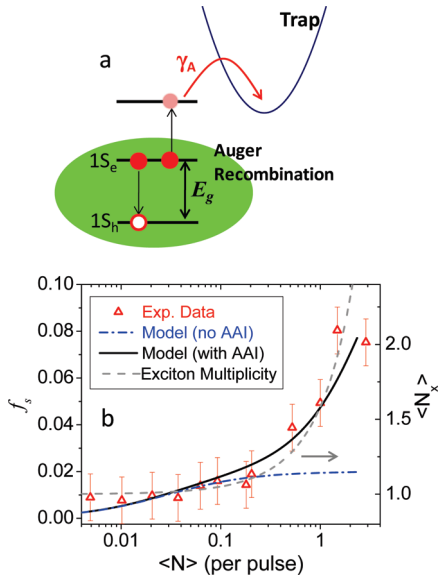

Figure 6. (a) Schematic representation of Auger-assisted ionization (referenced in the figure as AAI), the processes in which the ejection of a charge from the NQD is facilitated by Auger recombination. (b) Steady-state fraction of charged nanocrystals (open red triangles) as a function of initial NQD occupancy, $\langle N \rangle$, in the case of high-intensity excitation with 200 fs, 800 nm pulses when $\langle N \rangle$ reaches a value as high as ~3; PbSe NQDs with $E_g = 0.76$ eV. The growth of f_s at high pump levels correlates with the increase of the exciton multiplicity, $\langle N_x \rangle$ (shown by gray dashed line), suggesting that it is likely due to AAI. The black line is a fit to the model, which accounts for AAI (see text for details). The calculations without accounting for this process are shown by the blue dashed-dotted line.

To analyze the relative contribution from Auger-assisted ionization to photocharging, we have conducted a study of photoionization in the regime of short-pulse excitation with low-energy photons ($\hbar\omega < E_{th2}$) but high per-pulse fluences where the average NQD occupancy ($\langle N \rangle$) reaches values greater than unity. The results of this study are shown in Figure 6b (PbSe NQD sample with E_g = 0.76 eV), where f_s is plotted as a function of $\langle N \rangle$ (open red triangles); the sample is excited at 1.5 eV by 200 fs pulses derived from an amplified femtosecond laser operating at the repetition rate υ = 250 kHz. At low pump fluences ($\langle N \rangle < 0.3$), we observe only a small variation in f_s in the range 0.01−0.02. However, as $\langle N \rangle$ approaches unity, the degree of photocharging rapidly increases, and this increase correlates with the growth of exciton multiplicity, $\langle N_x \rangle = \langle N \rangle/(1 - p_0)$ (dashed gray line in Figure 6b), calculated assuming a Poisson distribution of NQD occupancies: $p_n = (\langle N \rangle^n/n!) \exp(-\langle N \rangle)$.[31] This behavior is consistent with Auger-assisted ionization. We can further quantitatively model it by introducing an additional term in the right-hand side of eq 1 to account for photoionization *via* Auger decay of multiexcitons. We present this term as $\nu f_{0A} \sum_{n=2}^{\infty} \gamma_A (n-1) p_n = \nu f_{0A} \gamma_A (\langle N \rangle - 1 + p_0)$, where we assume that the probability of Auger-assisted photocharging scales linearly with the number of Auger decay events (1 for a biexciton, 2 for a triexciton, *etc.*; γ_A is the probability per single event) and the maximum fraction of dots that can be "charged" by the Auger process, f_{0A}, is equal to f_0 measured for a hot-carrier excited by E_g above the band-edge (*i.e.*, is excited near the threshold for strong ionization). In the case of mirror-symmetric conduction and valence bands this would correspond to $\hbar\omega = 3E_g$ and, hence, $f_{0A} = f_0|_{\hbar\omega = 3Eg}$.

By modeling the results in Figure 6b (solid black line), we obtain that γ_A is 1.0×10^{-6} for $f_{0A} = 0.16$. The value of γ_A derived from the fit is comparable to the photoionization probability measured for 1.5 eV but considerably smaller than that observed in the regime of low-intensity excitation with $3E_g$ photons ($\gamma = 1.3 \times 10^{-5}$). This implies that while Auger-assisted processes might indeed contribute to photocharging, the magnitude of this contribution seems to be smaller than that due to direct hot-electron transfer. Therefore, a close correspondence between the spectral onset of CM and the threshold for strong photocharging (E_{th2}) is likely coincidental, and therefore, photoionization observed in our experiments is dominated by hot-carrier processes and not CM across the entire range of spectral energies (including the region above E_{th2}). While this assessment is still preliminary and requires further quantitative studies, it still calls for special caution in cases in which conclusions on the presence of CM and its efficiency are drawn solely from spectral dependences without quantitative measurements of CM yields.

CONCLUSIONS

We have conducted the study of photocharging in PbS and PbSe NQD solutions as a function of energy of the excitation photon. Our measurements reveal the existence of two spectral thresholds that mark the onsets of weak (E_{th1}) and strong (E_{th2}) photoionization. The studies of NQDs of different sizes (*i.e.*, different band gaps) show direct correlations between both of these thresholds and E_g. This observation indicates that the onsets for weak and strong ionization are associated with excitation of specific NQD states (tentatively ascribed to 1P and 2P, respectively) and are not significantly dependent on the energy of the acceptor state outside the nanocrystal. This situation is unusual from the point of view of traditional ionization, where the ionization energy is defined by the energy separation between the initial NQD state and the final external acceptor state and is not directly linked to E_g.

The exact nature of observed ionization thresholds still requires further studies. They may develop as a result of ejection of two different types of carriers (an electron and a hole, as suggested by a comparative study of core-only and core/shell samples) or from the existence of two distinct types of acceptor sites for the same carrier. We have also analyzed the possibility that the second threshold, which is near the onset for

multiexciton generation, develops as a result of Auger-assisted ionization of multiexcitons produced by CM. Our initial assessment, however, is that the contribution from CM to photoionization is considerably smaller than that due to direct hot-carrier transfer.

We have also conducted a study of NQD size-dependent lifetimes, τ_{eh}, of charge-separated states produced by photoionization and observe that τ_{eh} decreases with decreasing NQD size or, correspondingly, increasing band gap energy. Using the configuration-coordinate formalism, this observation can be explained as being due to a decrease in the potential barrier to back transfer of a trapped charge to the NQD.

On the basis of spectrally dependent measurements of the degree of photocharging and the results of lifetime studies we derive the spectral dependence of photoionization probabilities. We universally observe a quick increase of γ with $\hbar\omega$, typically over almost 2 orders of magnitude for photon energies between 1.5 and 3.5 eV; however, the absolute values of γ differ widely from one NQD sample to the next, ranging from 10^{-6} to 10^{-3} at 1.5 eV and from 10^{-4} to 10^{-1} at 3.5 eV. Potential sources of sample-to-sample variations in γ might include systematic size-dependent trends due to increasing leakage of electronic wave functions outside the nanocrystal for smaller NQD sizes as well as variations in surface/interface properties. Because of the latter factor, γ might vary even among nominally identical samples of the same NQD size due to minute differences in synthesis and handling of the nanocrystals that can lead to uncontrolled changes in surface chemistry through, for example, ligand loss or oxidation. This can affect the number and/or identity of specific acceptor sites involved in photoionization.

The present studies have direct relevance to two areas of current active research: CM and hot-electron transfer/extraction. The fact that the spectral dependence of photoionization probabilities mimics that expected for CM re-emphasizes the importance of a careful analysis of the influence of photocharging on results of quantitative measurements of CM efficiencies in the case of both spectroscopic studies of this effect as well as photocurrent and photoconductive gain measurements.

Recently, NQDs have been considered as a promising platform for the practical realization of concepts of hot-electron photovoltaic cells.[14] Specifically, a recent report by Tisdale *et al*. demonstrated the possibility of ultrafast, sub-ps extraction of hot carriers from PbSe nanocrystals.[13] In addition to characteristic time scales, an important parameter in the problem of hot-carrier transfer is the probability of charge ejection. The studies of photoionization described here indicate that this probability may be quantified *via* relatively straightforward measurements of photocharging. Further, our measurements indicate that the probability of hot-carrier transfer can be very high (~10%) even in the case of uncontrolled acceptor sites unintentionally incorporated into the ligand shell. This probability can clearly be even higher in the case of rationally designed acceptors with optimized energies and wave function overlaps.

METHODS

Sample Preparation. The samples investigated in this study are high-quality PbSe, PbSe/CdSe core/shell and PbS NQDs with band gaps ranging from 0.75 to 1.18 eV. PbSe and PbS/CdSe NQDs were synthesized by the methods described in ref 32, and were used without modification of their native oleic acid passivation. PbS NQDs were synthesized by the method of ref 33, then subjected to ligand exchange by overnight stirring in neat oleylamine at room temperature prior to spectroscopic study. In order to prevent uncontrolled changes to the NQD surfaces during the course of our spectroscopic measurements, the NQDs are dispersed in a nonpolar solvent and loaded into 1 mm path-length cuvettes in an Ar-filled glovebox. The solvents used in this study include toluene, chloroform, hexane, and trichloroethylene. We have not observed any appreciable effect of solvent identity on results of the measurements.

Spectral Dependence of Photocharging. Photocharging is inferred from the suppression of PL caused by the formation of trions, which decay *via* Auger recombination.[8] By comparing PL of sample solutions with and without stirring (which precludes the accumulation of charged NQDs in the studied volume), we can obtain the degree of photocharging. The spectral dependence of photocharging is investigated by comparing stirred and static PL intensities of a given sample as a function of photon energy using a PL excitation setup with a tungsten or a xenon lamp as a light source. The lamp radiation is filtered by a monochromator with a 20 nm bandwidth and then focused onto the sample; the excitation spot is ~3 mm. The detection wavelength is selected with a second monochromator (~20 nm bandwidth), and the signal is detected with an InGaAs photodiode.

Charge-Separated State Lifetime Measurement. To directly measure the lifetimes of the charge-separated states on tens of seconds time scales, we implement two different experimental techniques. In one method, we record the evolution of the PL signal after stirring is abruptly stopped, as the PL intensity gradually diminishes due to accumulation of charged species. In the second method, we employ separate light sources to excite PL and induce photoionization. NQD emission is generated by weak "non-ionizing" near-infrared (near-IR) light in resonance with the lowest-energy 1S absorption feature from the spectrally filtered tungsten lamp. Photoionization is independently induced by more intense higher-frequency radiation (532 or 400 nm) from continuous-wave diode lasers. The near-IR excitation is mechanically chopped (25 Hz), which allows us to use a lock-in amplifier to reject emission generated by the ionization source. In this method, the lifetime of charged species and the level of photocharging are derived from the slow PL time transients (laboratory time frame) recorded after blocking the ionization source. The advantage of this second method is that it allows us to control the fraction of photoexcited NQDs and the degree of ionization within the excited NQD ensemble independently. It also can be applied to NQDs in solid-state matrices and NQD films where such means as stirring cannot be used to remove charged nanocrystals from the excited volume.

Auger-Assisted Ionization Measurement. To study the influence of Auger-assisted ionization, we excite the sample with 1.5 eV,

200 fs (FWHM) pulses from a Ti:Sapphire regenerative amplifier (RegA, Coherent, Inc.) operating at 250 kHz.

Acknowledgment. We thank Richard D. Schaller for help with setting up the system for infrared PLE measurements. V.I. K, I.R., P.N., D.C.L., and J.M.P. acknowledge support of the Center for Advanced Solar Photophysics, an Energy Frontier Research Center, funded by the U.S. Department of Energy (DOE), Office of Science, Office of Basic Energy Sciences. L.A.P. is supported by the Los Alamos National Laboratory LDRD program.

REFERENCES AND NOTES

1. Ghanassi, M.; Schanneklein, M. C.; Hache, F.; Ekimov, A. I.; Ricard, D.; Flytzanis, C. Time-Resolved Measurements of Carrier Recombination in Experimental Semiconductor-Doped Glasses: Confirmation of the Role of Auger Recombination. *Appl. Phys. Lett.* **1993**, *62*, 78–80.
2. Nirmal, M.; Dabbousi, B. O.; Bawendi, M. G.; Macklin, J. J.; Trautman, J. K.; Harris, T. D.; Brus, L. E. Fluorescence Intermittency in Single Cadmium Selenide Nanocrystals. *Nature* **1996**, *383*, 802–804.
3. Efros, A. L.; Rosen, M. Random Telegraph Signal in the Photoluminescence Intensity of a Single Quantum Dot. *Phys. Rev. Lett.* **1997**, *78*, 1110–1113.
4. Klimov, V. I.; Mikhailovsky, A. A.; McBranch, D. W.; Leatherdale, C. A.; Bawendi, M. G. Quantization of Multiparticle Auger Rates in Semiconductor Quantum Dots. *Science* **2000**, *287*, 1011–1013.
5. McGuire, J. A.; Joo, J.; Pietryga, J. M.; Schaller, R. D.; Klimov, V. I. New Aspects of Carrier Multiplication in Semiconductor Nanocrystals. *Acc. Chem. Res.* **2008**, *41*, 1810–1819.
6. McGuire, J. A.; Sykora, M.; Joo, J.; Pietryga, J. M.; Klimov, V. I. Apparent Versus True Carrier Multiplication Yields in Semiconductor Nanocrystals. *Nano Lett.* **2010**, *10*, 2049–2057.
7. Midgett, A. G.; Hillhouse, H. W.; Hughes, B. K.; Nozik, A. J.; Beard, M. C. Flowing Versus Static Conditions for Measuring Multiple Exciton Generation in PbSe Quantum Dots. *J. Phys. Chem. C* **2010**, *114*, 17486–17500.
8. McGuire, J. A.; Sykora, M.; Robel, I.; Padilha, L. A.; Joo, J.; Pietryga, J. M.; Klimov, V. I. Spectroscopic Signatures of Photocharging Due to Hot-Carrier Transfer in Solutions of Semiconductor Nanocrystals Under Low-Intensity Ultraviolet Excitation. *ACS Nano* **2010**, *4*, 6087–6097.
9. Krauss, T. D.; Brus, L. E. Charge, Polarizability, and Photoionization of Single Semiconductor Nanocrystals. *Phys. Rev. Lett.* **1999**, *83*, 4840–4843.
10. Krauss, T. D.; O'Brien, S.; Brus, L. E. Charge and Photoionization Properties of Single Semiconductor Nanocrystals. *J. Phys. Chem. B* **2001**, *105*, 1725–1733.
11. Li, S.; Steigerwald, M. L.; Brus, L. E. Surface States in the Photoionization of High-Quality CdSe Core/Shell Nanocrystals. *ACS Nano* **2009**, *3*, 1267–1273.
12. Pandey, A.; Guyot-Sionnest, P. Hot Electron Extraction from Colloidal Quantum Dots. *J. Phys. Chem. Lett.* **2009**, *1*, 45–47.
13. Tisdale, W. A.; Williams, K. J.; Timp, B. A.; Norris, D. J.; Aydil, E. S.; Zhu, X. Y. Hot-Electron Transfer from Semiconductor Nanocrystals. *Science* **2010**, *328*, 1543–1547.
14. Ross, R. T.; Nozik, A. J. Efficiency of Hot-Carrier Solar Energy Converters. *J. Appl. Phys.* **1982**, *53*, 3813–3818.
15. Green, M. A. Third Generation Photovoltaics: Advanced Solar Energy Conversion. *Springer Series in Photonics* 2003.
16. Lee, D. C.; Robel, I.; Pietryga, J. M.; Klimov, V. I. Infrared-Active Heterostructured Nanocrystals with Ultralong Carrier Lifetimes. *J. Am. Chem. Soc.* **2010**, *132*, 9960–9962.
17. De Geyter, B.; Justo, Y.; Moreels, I.; Lambert, K.; Smet, P. F.; Van Thourhout, D.; Houtepen, A. J.; Grodzinska, D.; Donega, C. M.; Meijerink, A.; *et al*. The Different Nature of Band Edge Absorption and Emission in Colloidal PbSe/CdSe Core/Shell Quantum Dots. *ACS Nano* **2011**, *5*, 58–66.
18. Kang, I.; Wise, F. W. Electronic Structure and Optical Properties of PbS and PbSe Quantum Dots. *J. Opt. Soc. Am. B* **1997**, *14*, 1632–1646.
19. Franceschetti, A.; Luo, J. W.; An, J. M.; Zunger, A. Origin of One-Photon and Two-Photon Optical Transitions in PbSe Nanocrystals. *Phys. Rev. B* **2009**, *79*, 241311.
20. Bartnik, A. C.; Efros, Al.L.; Koh, W.-K.; Murray, C. B.; Wise, F. W. Electronic States and Optical Properties of PbSe Nanorods and Nanowires. *Phys. Rev. B* **2010**, *82*, 195313.
21. Nootz, G.; Padilha, L. A.; Olszak, P. D.; Webster, S.; Hagan, D. J.; Van Stryland, E. W.; Levina, L.; Sukhovatkin, V.; Brzozowski, L.; Sargent, E. H. Role of Symmetry Breaking on the Optical Transitions in Lead-Salt Quantum Dots. *Nano Lett.* **2010**, *10*, 3577–3582.
22. Sercel, P. C. Multiphonon-Assisted Tunneling Through Deep Levels: A Rapid Energy-Relaxation Mechanism in Nonideal Quantum-Dot Heterostructures. *Phys. Rev. B* **1995**, *51*, 14532–14541.
23. Califano, M. Direct and Inverse Auger Processes in InAs Nanocrystals: Can the Decay Signature of a Trion be Mistaken for Carrier Multiplication?. *ACS Nano* **2009**, *3*, 2706–2714.
24. Tyagi, P.; Kambhampati, P. False Multiple Exciton Recombination and Multiple Exciton Generation Signals in Semiconductor Quantum Dots Arise from Surface Charge Trapping. *J. Chem. Phys.* **2011**, *134*, 094706.
25. Beard, M. C.; Midgett, A. G.; Hanna, M. C.; Luther, J. M.; Hughes, B. K.; Nozik, A. J. Comparing Multiple Exciton Generation in Quantum Dots to Impact Ionization in Bulk Semiconductors: Implications for Enhancement of Solar Energy Conversion. *Nano Lett.* **2010**, *10*, 3019–3027.
26. Chepic, D. I.; Efros, Al.L.; Ekimov, A. I.; Ivanov, M. G.; Kharchenko, V. A.; Kudriavtsev, I. A.; Yazeva, T. V. Auger Ionization of Semiconductor Quantum Drops in a Glass Matrix. *J. Lumin.* **1990**, *47*, 113–127.
27. Peterson, J. J.; Nesbitt, D. J. Modified Power Law Behavior in Quantum Dot Blinking: A Novel Role for Biexcitons and Auger Ionization. *Nano Lett.* **2009**, *9*, 338–345.
28. Klimov, V. I.; McBranch, D. W. Auger-Process-Induced Charge Separation in Semiconductor Nanocrystals. *Phys. Rev. B* **1997**, *55*, 13173–13179.
29. Kraus, R. M.; Lagoudakis, P. G.; Müller, J.; Rogach, A. L.; Lupton, J. M.; Feldmann, J.; Talapin, D. V.; Weller, H. Interplay between Auger and Ionization Processes in Nanocrystal Quantum Dots. *J. Phys. Chem. B* **2005**, *109*, 18214–18217.
30. Sukhovatkin, V.; Hinds, S.; Brzozowski, L.; Sargent, E. H. Colloidal Quantum-Dot Photodetectors Exploiting Multiexciton Generation. *Science* **2009**, *324*, 1542–1544.
31. Klimov, V. I. Optical Nonlinearities and Ultrafast Carrier Dynamics in Semiconductor Nanocrystals. *J. Chem. Phys. B* **2000**, *104*, 6112–6123.
32. Pietryga, J. M.; Werder, D. J.; Williams, D. J.; Casson, J. L.; Schaller, R. D.; Klimov, V. I.; Hollingsworth, J. A. Utilizing the Lability of Lead Selenide to Produce Heterostructured Nanocrystals with Bright, Stable Infrared Emission. *J. Am. Chem. Soc.* **2008**, *130*, 4879–4885.
33. Hines, M. A.; Scholes, G. D. Colloidal PbS Nanocrystals with Size-Tunable Near-Infrared Emission: Observation of Post-Synthesis Self-Narrowing of the Particle Size Distribution. *Adv. Mater.* **2003**, *15*, 1844–1849.